Graphene and Doped Graphene: A Comparative DFT Study

Jyoti Tyagi, Lekha Sharma, Rita Kakkar*

Computational Chemistry Laboratory, Department of Chemistry, University of Delhi, Delhi, 110007, India

*Corresponding author: Tel: (+91) 11-27666313; E-mail: rkakkar@chemistry.du.ac.in

Received: 11 June 2018, Revised: 11 June 2018 and Accepted: 15 June 2018

DOI: 10.5185/amlett.2019.2168
www.vbripress.com/aml

Abstract

Two different models, ovalene ($C_{32}H_{14}$) and circumcoronene ($C_{54}H_{18}$) and their respective doped models ($C_{31}XH_{14}$, $C_{53}XH_{18}$ where X = B, Al, N, P, Fe, Ni and Pt) have been considered for DFT calculations at the GGA-PBE/DNP level. The two models are compared on the basis of various calculated structural parameters and electronic properties. Electronic density of states (DOS) spectra are also plotted to see the changes in the electronic properties on increasing the size. No major changes are observed in the structural and electronic properties as one move from the smaller model to the higher one. It is found that doping maintains the planarity of the surface but induces comparatively large changes in the bond lengths around the doped atom, weakening the bonds. Copyright © VBRI Press.

Keywords: DFT, graphene, doping, DOS.

Introduction

Graphene, two-dimensional graphite, is a zero-gap semiconductor. The robust two-dimensional structure of graphene makes it an exciting material for applications in the present era. Single-layer graphene is a one-atom thick sheet of sp^2-carbon atoms, densely packed into a two-dimensional honeycomb lattice. It is the mother of all graphitic forms of carbon, including zero-dimensional fullerenes, one-dimensional carbon nanotubes and three-dimensional graphite [**1**]**.** The graphene sheet is either doped by different elements, [**2-4**] or various elements are adsorbed on its surface at different positions [**5-13**] to see the effects on its electronic and magnetic properties.

Theoretically, graphene is represented by a range of models. $C_{24}H_{12}$, $C_{32}H_{14}$, $C_{42}H_{16}$, $C_{54}H_{18}$ and $C_{96}H_{24}$ models have been studied extensively for different applications in past as well as recent times [**14-23**]. A number of research groups have considered periodic structures with different dimensions to represent the graphene surface [**24-35**] to study the interaction with different chemical species. It has been previously shown that the reactivity of the carbon model does not depend strongly on the molecular size [**36**].

The present study is aimed at investigating the effect of doping on the structural and electronic properties of graphene and how these vary with the size of the sheet. For this purpose, two models were considered, $C_{32}H_{14}$ and $C_{54}H_{18}$ (intrinsic), and their respective doped models ($C_{31}XH_{14}$, $C_{53}XH_{18}$ where X = B, Al, N, P, Fe, Ni and Pt).

Computational details

First-principles density functional (DF) calculations were performed using DMol [**3]** in the Materials Studio 4.4 package from Accelrys Inc. [**37, 38]** Numerical basis sets of double zeta quality plus polarization functions (DNP), which is the numerical equivalent of the Gaussian basis, 6-31G**, but is much more accurate, were used in the calculations. The cores were treated using DFT Semilocal Pseudo-Potentials (DSPP), specifically designed for DFT calculations [**39**]. The GGA-PBE functional [**40**] was employed in the calculations. The geometries of various structures were fully optimized, without restrictions, using delocalized internal coordinates [**41, 42**]. The geometry optimization was performed until the magnitude of the Hellmann-Feynman force on each atom reduced to within 0.004 Ha $Å^{-1}$ and the energy change was less than 2×10^{-5} Ha. Self-consisted field procedure was carried out with a convergence criterion of 10^{-5} Ha on the energy. For the transition metal doped systems, which are open-shell systems, spin unrestricted calculations were performed [**43, 44]** on the low spin states of the metals. Bond orders were computed using Mayer's procedure [**45**]. Because of the well-known shortcomings of the Mulliken method, [**46**] molecular electrostatic potential (ESP) fitted charges, [**47**] which are consistent and basis size independent, are reported.

Results and discussion

Two models of intrinsic graphene, viz. ovalene, $C_{32}H_{14}$ and circumcoronene, $C_{54}H_{18}$ and their respective doped models ($C_{31}XH_{14}$, $C_{53}XH_{18}$, where X = B, Al, N, P, Fe, Ni and Pt) were considered for the present study. The number of fused benzene rings in the $C_{32}H_{14}$ and $C_{54}H_{18}$ models is 10 and 19, respectively. The central carbon atom was doped in the two models of graphene. Doping of graphene with B and Al was done to investigate the effect of *p*-type doping, and with N and P to study *n*-type doping. Other than these four elements, three transition metal elements (Fe, Ni and Pt) were chosen for doping because fruitful results have been reported [**25-27]** for adsorption of chemical species when doping was done with these elements.

Graphene model-Ovalene ($C_{31}XH_{14}$)

All the considered graphene models, intrinsic as well as doped (B, Al, N, P, Fe, Ni and Pt), were fully optimized with respect to the energy. The structure of doped graphene is shown in **Fig. 1**, along with the numbering scheme.

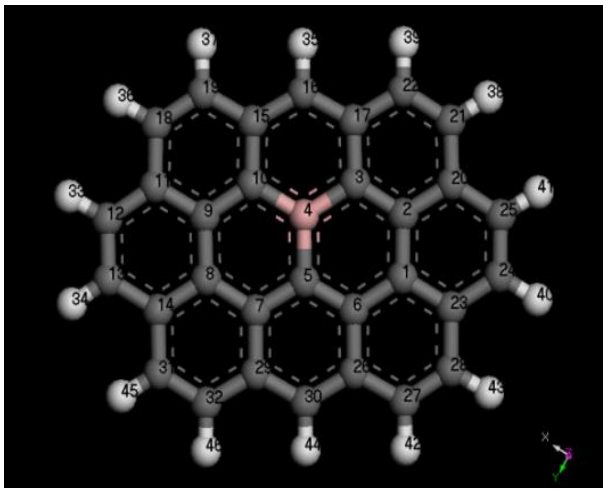

Fig. 1 Optimized structure of the graphene model ($C_{31}XH_{14}$). Gray, peach and white spheres denote C, X and H, respectively.

Structural properties

The calculated average C-C and C-H bond lengths for intrinsic graphene (**Table 1**), compare well with the reported values of 1.420 Å for C-C [**24, 48**] and 1.09 Å for C-H [**49**]. The Handbook of Chemistry (67th ed.; CRC Press: Cleveland, OH, 1978; p F158) lists these values as 1.42 Å and 1.07 Å, respectively. On doping with the various atoms, the average C-X bond lengths get modified, as shown in **Table 1**, and these values are in good agreement (within 10%) with the values reported in the literature, i.e. C-B = 1.481 Å, [**28**] C-Al = 1.633 Å [**24**], C-N = 1.408 Å, [**28**] C-P = 1.765 Å, [**50**] and C-Pt = 1.92 Å [**26**]. Except N, in each case, the C-X bond lengthens due to the larger atomic radius of the doped atom as compared to carbon. The increased bond lengths induce greater reactivity in graphene, which can be used for various future applications. The maximum increase (0.406 Å) in bond length is observed for the Pt-graphene system, which suggests greatest reactivity in this system. The increase in reactivity is also supported by the other structural and electronic parameters, discussed in the following sections.

Table 1. Calculated gas phase bond lengths (Å) and bond angles (°) of the graphene models.

X	C	B	Al	N	P	Fe	Ni	Pt
Bond lengths (Å)								
X4-C3	1.418	1.500	1.764	1.417	1.655	1.712	1.716	1.826
X4-C5	1.430	1.497	1.765	1.405	1.649	1.720	1.730	1.831
X4-C10	1.418	1.500	1.764	1.417	1.655	1.712	1.716	1.826
Average	1.422	1.499	1.764	1.413	1.653	1.715	1.721	1.828
Bond angles (°)								
C3X4C5	120.0	119.9	119.9	120.0	119.9	120.1	112.9	119.4
C3X4C10	120.0	120.1	120.2	120.0	120.2	119.7	134.1	121.1
C5X4C10	120.0	119.9	119.9	120.0	119.9	120.1	112.9	119.4

A look at **Table 1** reveals that the bond angles around the doped atom remain close to the carbon sp^2 bond angle of 120.0° that it replaces, except in the case of Ni, where the bond angles deviate appreciably, though the planar geometry is still retained.

Electronic properties

The Mayer bond orders **(Table 2)** for the C-C bonds in intrinsic graphene are of the order ~1.2, confirming sp^2 hybridization for the carbon atoms. The C-H bond orders are all ~1.0, and there is no significant change in the doped models. However, some significant changes are observed in the Mayer bond orders for the three C-X bonds around the doped atom. Significant weakening of the C-X bonds results upon doping, particularly in the case of doping with Al. The only exception is P-doping. While the X4-C5 bond is weaker than the other two X-C bonds for intrinsic graphene, the opposite trend is observed in all cases, except for Fe doping.

Table 2. Mayer bond orders for the various graphene models ($C_{32}H_{14}$ and $C_{31}XH_{14}$).

Bond*	X							
	C	B	Al	N	P	Fe	Ni	Pt
C2C3	1.195	1.246	1.298	1.247	1.203	1.175	1.202	1.128
C3X4	1.214	1.003	0.789	1.061	1.205	1.213	0.929	1.131
X4C5	1.165	1.018	0.794	1.085	1.239	1.180	1.082	1.151
C5C6	1.213	1.245	1.313	1.239	1.188	1.208	1.213	1.140
C5C7	1.214	1.243	1.314	1.240	1.190	1.209	1.213	1.141
X4C10	1.213	1.004	0.790	1.061	1.206	1.213	0.924	1.131
C9C10	1.196	1.243	1.298	1.247	1.204	1.176	1.201	1.128
C10C15	1.158	1.207	1.280	1.204	1.172	1.167	1.138	1.082
C3C17	1.158	1.208	1.280	1.204	1.173	1.167	1.137	1.082

*See Fig. 1.

ESP charge analysis (Table S1) for the intrinsic graphene shows that the inner C atoms bear negligible charges, but the terminal carbon atoms (C16 and C30, see Fig. 1) are negatively charged, due to transfer of electron density from their neighboring carbons (C15, C17 and C26, C29, see Fig. 1), which are positively charged. On doping, except with Ni and Pt, the doped atom acquires a positive charge due to electron transfer to the rest of the graphene sheet. As noted above, Al, in particular, forms weak covalent bonds with its neighboring carbons. The larger positive charge on Al in the doped system implies that the Al-C bonds have ionic character as well. This is borne out by the almost mononegative charges (~ -0.8) on the three carbons (C3, C5, and C10) to which it is bound. The electronegativity values for C, B, Al, N and P are 2.54, 2.04, 1.61, 3.04 and 2.19, respectively [**51**]. The large difference in the electronegativities of C and Al explains the ionic character of the Al-C bond. The polarity of the C-X bond is in the order of the electronegativity difference of C and X, the maximum positive charge being on Al, followed by P and then on B. Aluminum also induces a polarization in all the bonds, as seen by the large partial charges on nearly all the atoms of the Al doped system. On the other hand, the d^8 transition metals, Ni and Pt, show their electrophilic character [**52-54**] by withdrawing electron density from the graphene. However, the electron withdrawal is smaller than the electron donation by Al and not much change occurs in the partial charges of the bonded carbons.

The charge redistribution on doping causes a change in the dipole moment from zero for intrinsic graphene to significant values in the doped systems (Table S2). Even though most atoms in the Al doped graphene bear significant charges, the dipole moment remains small. However, Pt-graphene has the highest dipole moment, showing greater asymmetry in the charge distribution. P and Fe also induce dipole moments in graphene. Both charge transfer and dipole moment support the notion that doping influences the electronic properties of graphene.

The binding energies per atom, given in Table S2, indicate a destabilization of the graphene, and consequent increase in reactivity, on doping, the largest destabilization being observed for doping with Pt, and the least for doping with boron. The energy difference between the lowest unoccupied molecular orbital (LUMO) and the highest occupied molecular orbital (HOMO) decreases substantially on doping, again indicating greater reactivity of the doped systems. However, the decrease is relatively smaller in the case of Pt doping. Among the *n*-type (N, P) and *p*-type (B, Al) dopants, the decrease in band gap is larger in the former than in the latter. The decreased band gap indicates increase in conductivity of the graphene on doping. The calculated Fermi energies, also given in Table S2, indicate that doping increases the Fermi energy of intrinsic graphene (a closed shell system), except for Al for which the Fermi level goes down. The maximum increase in the Fermi level is for the *n*-type dopants (N and P), suggesting easy conduction of electrons in these two sheets. Increase in the Fermi energy of the doped systems also reflects a greater occupation of graphene energy states.

The magnetic moments of the isolated atom (μ_A), doped atom in the graphene sheet (μ_{DA}) and doped graphene sheet (μ_{DG}) (Table S2), calculated from the Mayer free valences, show that the doped graphene sheets become magnetic on doping, except for Pt-graphene, in which case, even though the isolated Pt atom has a magnetic moment of 1.96 μ_B, the magnetism gets quenched in the sheet. Further, the magnetic moment of the atom, when in the graphene sheet, is always smaller than that in the isolated atom, suggesting transfer of electrons to the graphene sheet. This reduction in magnetic moment is most for *n*-doped graphene, signifying greater electron transfer to the sheet as compared to other systems. The induction of magnetism in the graphene sheet on doping has also been experimentally observed.[55]

We may understand the process of doping thus. When a carbon atom is removed from the hexagonal network, three C atoms (C3, C5 & C10 in Fig. 1) are left with one unsaturated bond each. After relaxation, the single vacancy undergoes a Jahn–Teller distortion, where two of the unsaturated C atoms form a weak covalent bond, resulting in a pentagonal rearrangement, whereas the remaining unsaturated C atom has a magnetic moment of 0.88 μ_B. The X atom forms covalent bonds with the under-coordinated C atoms at the vacancy by breaking the weak C–C bond of the pentagon in the reconstructed vacancy. This means that doping in graphene could be created easily by depositing X atoms where vacancies have been previously created by, for example, irradiation with energetic electrons. However, instead of zero magnetic moment, the magnetic moment of the substitutional X impurity increases.

The HOMO and LUMO orbitals are important, both in shape and magnitude, as they account for the chemical reactivity of a molecule. The HOMO-LUMO plots are shown in Table S3. It can be seen that all the LUMO energies are negative, which implies that the systems under investigation are all good electron acceptors. The decrease in the HOMO-LUMO gap on doping is also due to the lowering of the LUMO.

Concentrating on the doped atom, Table S3 shows that, in intrinsic graphene, both the HOMO and LUMO are π orbitals. While the HOMO is a delocalized orbital involving the two equivalent bonds, X4-C3 and X4-C10 (**Fig. 1**), the LUMO is the X4-C5 π* bond orbital. In *p*-type doping, both the HOMO and LUMO lie on the doped atoms and both are delocalized π orbitals on X4-C3 and X4-C10. For *n*-type doping, however, both are π* orbitals encompassing X4-C3 and X4-C10, but

for P, both the HOMO and LUMO are additionally stabilized by π bonding involving X4-C5. In the case of Fe doping, all three are π* orbitals, both for the HOMO and LUMO. In all these cases, the similarity of the HOMOs and LUMOs explains the decreased gaps. However, for Ni and Pt doping, while the former dopant does not appear in the LUMO, the latter does not appear in the HOMO, accounting for the increased band gap in the case of the Pt-doped system, where the metal orbitals do not mix with the HOMO to destabilize it.

The total density of states (DOS) spectra (spin-up and spin-down) for all the models are plotted in **Fig. 2** to analyze the variations in the electronic and magnetic properties on doping.

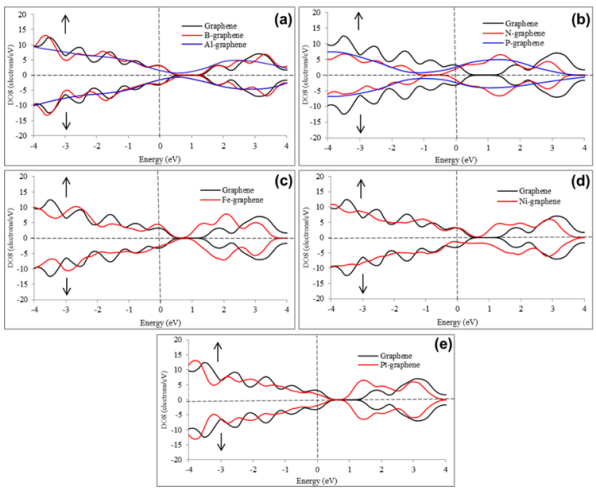

Fig. 2. The spin-up (↑) and spin-down (↓) density of states (DOS) of intrinsic graphene (black) with: (a) B-graphene (red), Al-graphene (blue) (b) N-graphene (red), P-graphene (blue) (c) Fe-graphene (red) (d) Ni-graphene (red) (e) Pt-graphene (red). The vertical dashed line denotes the Fermi level

Intrinsic graphene is a non-magnetic material, and this is reflected in the symmetry of the spin-up and spin-down DOS **(Fig. 2(a))**. B and Al dopants introduce electronic holes in the intrinsic graphene, generating *p*-type semiconductors. For B-graphene, there is a slight shift in the peaks of the spin-down state towards high energy above the Fermi level as compared to the spin-up state **(Fig. 2(a))**. The zero DOS level shifts to high energy above the Fermi level, as expected for *p*-type behavior [**28**]. The DOS curve for Al doping is smoother than that of intrinsic graphene, and the spin-up and spin-down curves are almost mirror images of each other. For both N and P doped graphene **(Fig. 2(b))** (*n*-type semiconductors), a shift of the zero DOS is observed towards energies lower than the Fermi level. For N-doping, there are significant differences in the spin-up and spin-down behavior near and above the Fermi level.

For the Fe and Ni doped graphene, considerable difference in the spin-up and spin-down curves is observed, accounting for high magnetic moments (Table S2). For the Fe- and Ni-doped graphene, the peaks for the spin-down DOS shift to higher energy as compared to those for spin-up. However, for Pt doping, although the zero DOS state is above the Fermi level, as for the Fe-doped graphene, the spin-up and spin-down curves are almost mirror images of each other, accounting for the zero magnetization of Pt-doped graphene. The difference in the magnetic behavior resulting from doping with Ni and Pt, both of which belong to the same group, can be explained on the basis of the Mulliken population analysis for the two systems. Though in the isolated state, Ni and Pt have the electron configurations $3d^8 4s^2$ and $5d^9 6s^1$, respectively, and both have intrinsic magnetic moments, in the graphene doped with the respective metals, the net configurations is $4s^{1.17} 3d^{8.78} 4p^{0.20}$ for Ni and $6s^{1.35} 5d^{8.33} 6p^{0.38}$ for Pt, revealing that, in the former, one electron is transferred from the 4*s* orbital to the 3d orbital, resulting in net α spin.

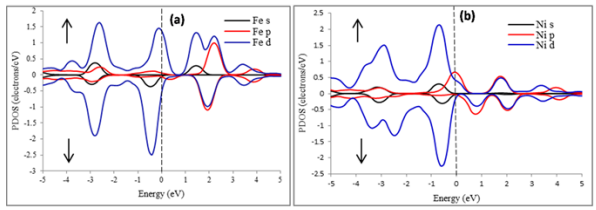

Fig. 3. The spin-up (↑) and spin-down (↓) PDOS of (a) Fe in Fe-graphene (b) Ni in Ni-graphene. The s, p and d orbitals are shown in black, red and blue, respectively.

For a better understanding of the magnetic behavior of Fe-graphene and Ni-graphene, the partial DOS (PDOS) of Fe in Fe-graphene and Ni in Ni-graphene were also analyzed. The PDOS of Fe in Fe-graphene is shown in **Fig. 3(a)**. The spin-up and spin-down s electrons of Fe in Fe-graphene differ in their DOS, as the latter have their peaks near -0.5 eV in the valence band, while the former peak near 1.5 eV in the conduction band. For the p electron states, both the spin-up and spin-down states contribute to the conduction band, and the respective peaks are at 2.2 eV and 1.9 eV. The peaks of the d electron states are higher and deeper in the valence band for the spin-down states, but the spin-up states make larger contribution to the conduction band. The PDOS suggests that there is hybridization between the 4s and 3d orbitals of the Fe atom, due to which the 4s and 3d spin-up states shift to the conduction band, as also seen from electron configuration of Fe ($4s^{1.06} 3d^{6.94} 4p^{0.18}$), showing a transfer of an electron from the s to the d orbitals.

The PDOS of Ni in Ni-graphene is shown in **Fig. 3(b)**. Though some variations are seen in the peak positions in the DOS for the spin-up and spin-down states for the s states, these are not very significant. Near the Fermi level, a peak for the spin-up p states at -0.08 eV in the valence band shifts to 0.75 eV in the conduction band for the spin-down states. Around 0.75 eV, the d electron spin-up state has zero DOS, but at the same level, the spin-down states have a peak. The opposite is the case around the Fermi level. Some mixing between the s, p and d orbitals leads to a

$4s^{1.17}3d^{8.78}4p^{0.20}$ configuration for Ni. The PDOS of Fe and Ni graphene are clearly different for spin-up and spin-down states, which confirms the magnetization of the sheet.

Higher graphene model-Circumcoronene ($C_{53}XH_{18}$)

For the larger model of graphene, doping was done with the same atoms as in the lower model, and all the structures of the considered graphene models were fully optimized. The structure of doped graphene is shown in **Fig. 4**.

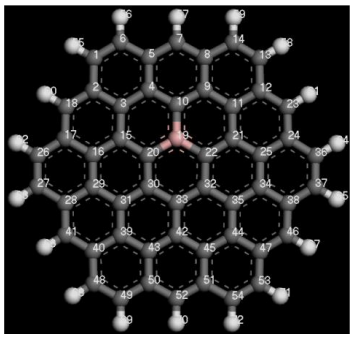

Fig. 4. Optimized structure of graphene model, $C_{53}XH_{18}$.

Structural properties

Selected bond lengths and bond angles in the optimized geometry of doped graphene are given in Table S4 of the Supporting Information. As observed in the smaller model of graphene (Table 1), there are significant changes in the bond lengths around the doped atom. The trend is similar to that observed in the smaller model. As before, no major change in the bond angles around the doped atom (C19) are observed, except in Ni-graphene.

The calculated Mayer bond orders are given in Table S5. Here, too, no significant changes are observed in the Mayer bond orders in the $C_{54}H_{18}$ model as compared to the $C_{32}H_{14}$ model.

Electronic properties

The ESP partial charges are listed in Table S6. Though there are slight differences in the charges on the doped atom for the larger model as compared to the smaller one (Table S1), the variations are slight and the same trends persist, as can be seen from **Fig. 5**.

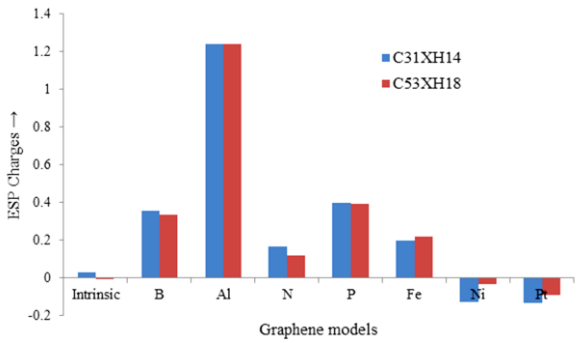

Fig. 5. Variation in the ESP charges on the doped atom for the lower and higher models of graphene.

The calculated electronic properties are given in Table S7. As for the smaller model, doping results in destabilization of the graphene, the binding energy per atom is found to be decreased in each doped case as compared to the intrinsic graphene (Fig. S1), the maximum destabilization being for Pt doping. The magnitude of the binding energy per atom is larger for the larger model, indicating stabilization of the system as one moves towards the larger model. The magnetic moments (Table S7) show the same trend as observed for the smaller model (Table S2), but the magnitudes are slightly smaller.

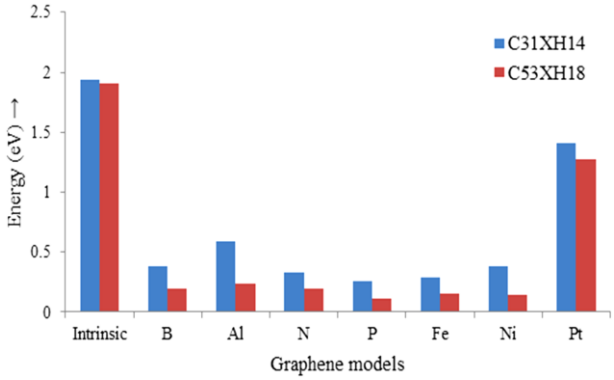

Fig. 6. Variation in band gap for lower and higher models of graphene.

A decrease in the HOMO-LUMO gap is observed for each larger model as compared to its respective smaller model **(Fig. 6)**. As for the smaller model, the band gap of intrinsic graphene decreases on doping. The calculated Fermi energy for intrinsic graphene is -4.56 eV and it is raised on doping (Table S7). This is in contrast to the observation for the smaller model, where the Fermi energy does not increase for *p*-doping. However, as before (Table S2), the shift of the Fermi level is largest for *n*-doping. The dipole moments of the doped sheets change to significant values (Table S7), signifying redistribution of charge among the atoms of the sheet. Compared to the smaller model (Table S2), the dipole moments for the B-, Al-, and N-doped graphene increase to very high values.

The HOMO-LUMO plots are shown in Table S8, along with their respective energies in eV. These are similar to those observed for the smaller model, except for the P and Pt-doped systems, where the doped atom does not find any contribution to the LUMO. For Ni doping, for which no contribution to the LUMO was found for the smaller model, for the larger model, it comprises the B1 π orbital, accounting for the drastic lowering of this level.

The total density of states (DOS) plots (spin-up and spin-down) for the larger models are plotted in Figure S2. Compared to the smaller model, the variations between the spin-up and spin-down curves is smaller, except for the Fe and Ni doped systems.

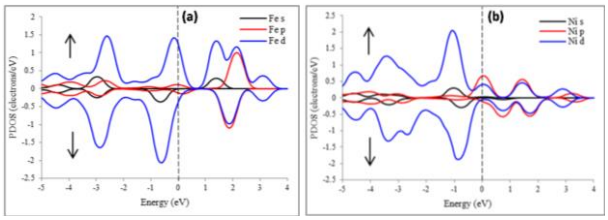

Fig. 7. The spin-up (↑) and spin-down (↓) PDOS of (a) Fe in Fe-graphene (b) Ni in Ni-graphene. The s, p and d orbitals are shown in black, red and blue, respectively.

As for the smaller model, the PDOS of Fe in Fe-graphene **(Fig. 7(a))** and Ni in Ni-graphene **(Fig. 7(b))** were analyzed. The PDOS of Fe in Fe-graphene shows similar variations in the spectra as for the smaller model, i.e. relatively large differences in the two spin states of the s electrons, small variations in the p electron states, and the d electron spin-up states split into two peaks above the Fermi level in the range of 1.3 and 2.4 eV. However, there are small changes in the PDOS of Ni in Ni-graphene as compared to the smaller model. At the Fermi level, the spin-up p electron states have a peak, while the spin-down states have almost zero density of states. This observation differs from that of the smaller model, which showed similar peaks for both the states around 0.7 eV. Also, the *d* electron spin-up states have a clear peak at the Fermi level, differing from the smaller model. The electron configurations of the Fe and Ni atoms in the larger sheet are $4s^{1.06}3d^{6.95}4p^{0.19}$ and $4s^{1.18}3d^{8.76}4p^{0.21}$, respectively. In each case, a 4s electron is promoted to the 3d orbital, along with some population of the 4p orbital.

Conclusion

In summary, our first-principles DFT calculations to study the structural, electronic and magnetic properties of intrinsic as well as doped graphene, have revealed significant changes in the structural properties (bond lengths, bond angles and Mayer bond orders) on doping, but these are not size-dependent on the model. On doping, the graphene sheet exhibits magnetism, except for Pt atom doping, and the magnitude of the magnetic moment depends on the doped atom. The magnitude of the binding energy per atom increases as the model becomes larger. The binding energy per atom decreases on doping, suggesting an increase in reactivity on doping, as also evidenced by the decrease in the band gap on doping. Charge redistribution is observed in the doped sheets, supported by the ESP charges on the atoms and the calculated dipole moments. The DOS plots of the graphene models show that intrinsic and Pt graphene are non-magnetic, while Fe and Ni doped graphene is magnetic. Interestingly, around the Fermi level, Al, P and Ni graphene exhibit non-zero density of states, while Fe-graphene has zero density of states. For the *p*-type dopants (B and Al), the DOS peaks move towards high energy, while for *n*-type dopants (N and P), they move towards low energy, as compared to intrinsic graphene.

Acknowledgements

The author Lekha Sharma acknowledges the financial support provided by CSIR, New Delhi in the form of Senior Research Fellowhip.

Author's contributions

Conceived the plan: JT; Performed the computations: JT; Data analysis: JT, RK; Wrote the paper: JT, RK, LS. Authors have no competing financial interests.

Supporting information

Supporting informations are available from VBRI Press.

References

(a) Scientific article

1. Tyagi, J.; Kakkar, R.; *Adv. Mater. Lett.*, 2013, *4*, 721.
2. Govindaraj, A.; Rao, C. N. R.; Doping of graphene by nitrogen, boron and other elements, In Functionalization of Graphene; Georgakilas, V. (Ed.); Wiley-VCH Verlag GmbH & Co., **2014**, pp. 283-358.
   Kong, X. K.; Chen, C. L.; Chen, Q. W.; *Chem. Soc. Rev.*, **2014**, *43*, 2841.
3. Rao, C. N. R.; Gopalakrishnan, K.; Govindaraj, A.; *Nano Today*, **2014**, *9*, 324.
4. Aktürk, E.; Ataca, C.; Ciraci, S.; *Appl. Phys. Lett.*, **2010**, *96*, 123112/1.
5. Chan, K. T.; Neaton, J. B.; Cohen, M. L.; *Phys. Rev. B*, **2008**, *77*, 235430/1.
6. Hu, L.; Hu, X.; Wu, X.; Du, C.; Dai, Y.; Deng, J.; *Physica B*, **2010**, *405*, 3337.
7. Tachikawa, H.; Nagoya, Y.; Fukuzumi, T.; *J. Power Sources*, **2010**, *195*, 6148.
8. Legesse, M.; Mellouhi, F. E.; Bentria, E. T.; Madjet, M. E.; Fisher, T. S.; Kais, S.; Alharbi, F. H.; *Appl. Surf. Sci.*, **2017**, *394*, 98.
9. Tran, N. T. T.; Dahal, D.; Gumbs, G.; Lin, M.-F.; *Struct. Chem.*, **2017**, *28*, 1311.
10. Tang, Y.; Zhang, H.; Shen, Z.; Zhao, M.; Li, Y.; Dai, X.; *RSC Adv.*, **2017**, *7*, 33208.
11. Kepaptsoglou, D.; Hardcastle, T. P.; Seabourne, C. R.; Bangert, U.; Zan, R.; Amani, J. A.; Hofsäss, H.; Nicholls, R. J.; Brydson, R. M. D.; Scott, A. J.; Ramasse, Q. M.; *ACS Nano*, **2015**, *9*, 11398.
12. Widjaja, H.; Altarawneh, M.; Jiang, Z.-T.; *Canadian Journal of Physics*, **2016**, *94*, 437.
13. Bauschlicher, C. W.; *Chem. Phys. Lett.*, **2016**, *665*, 100.
14. Ishimoto, T.; Koyama, M.; *J. Comput. Chem. Jpn.*, **2014**, *13*, 171.
15. Mocci, P.; Cardia, R.; Cappellini, G.; *J. Phys.: Conf. Series*, **2018**, *956*, 012020(1).
16. Mutoh, M.; Abe, S.; Kusaka, T.; Nakamuru, M.; Yoshida, Y.; Iida, J.; Tachikawa, H.; *Atoms*, **2016**, *4*, 4.
17. Owens, F. J.; *Mol. Phys.*, **2018**, *116*, 1275.
18. Medeiros, P. V. C.; Gueorguiev, G. K.; Stafström, S.; *Phys. Rev. B*, **2012**, *85*, 205423(1).
19. Ramraj, A.; Hillier, I. H.; Vincent, M. A.; Burton, N. A.; *Chem. Phys. Lett.*, **2010**, *484*, 295.
20. Song, K.; Long, Y.; Wang, X.; Zhou, G.; *Nano Res.*, **2018**, *11*, 254.
21. Wang, C.; Ding, Y. H.; *J. Mater. Chem. A*, **2013**, *1*, 1885.
22. Yatsymyrskyi, A. V.; Grishchenko, L. M.; Diyuk, V. E.; Zaderko, A. N.; Boldyrieva, O. Y.; Lisnyak, V. V.; *Nanomaterials: Application & Properties (NAP)*, **2017**.
23. Chi, M.; Zhao, Y. -P.; *Comp. Mater. Sci.*, **2009**, *46*, 1085.
24. Ding, N.; Lu, X.; Wu, C. -M. L.; *Comp. Mater. Sci.*, **2012**, *51*, 141.
25. Ma, F.; Zhang, Z.; Jia, H.; Liu, X.; Hao, Y.; Xu, B.; *J. Mol. Struct.: THEOCHEM*, **2010**, *955*, 134.
26. Zhang, K.; Dwivedi, V.; Chi, C.; Wu, J.; *J. Hazard. Mater.*, **2010**, *182*, 162.

27. Zhang, Y. H.; Yue, L. J.; Han, L. F.; Chen, J. L.; Fang, S. M.; Jia, D. Z.; Li, F.; *Computational and Theoretical Chemistry*, **2011**, *972*, 63.
28. Valencia, A. M.; Caldas, M. J.; *Phys. Rev. B*, **2017**, *96*, 125431.
29. Cavallucci, T.; Murata, Y.; Takamura, M.; Hibino, H.; Heun, S.; Tozzini, V.; *Carbon*, **2018**, *130*, 466.
30. Salmankurt, B.; Gürel, H. H.; *AIP Conference Proceedings*, **2017**, *1815*, 050012.
31. Romero, M. T.; Alvarado, Y. A.; Garcia-Diaz, R.; Garcia, C. R.; Valiente, R. O.; Cocoletzi, G. H.; *Nano Hybrids and Composites*, **2017**, *16*, 52.
32. Rekha, B.; Seenithurai, S.; Pandyan, R. K.; Kumar, S. V.; Mahendran, M.; *Nano hybrids and Composites*, **2017**, *17*, 131.
33. Silva, C. d.; Saiz, F.; Romero, D. A.; Amon, C. H.; *Phys. Rev. B*, **2016**, *93*, 125427.
34. Gupta, V.; Kumar, A.; Ray, N.; *AIP Conference Proceedings*, **2018**, *1953*, 140013.
35. Sheka, E. F.; Chernozatonskii, L. A.; *Int. J. Quantum Chem.*, **2010**, *110*, 1938.
36. Delley, B.; *J. Chem. Phys.*, **1990**, *92*, 508.
37. Delley, B.; *J. Chem. Phys.*, **2000**, *113*, 7756.
38. Delley, B.; *Phys. Rev. B*, **2002**, *66*, 155125/1.
39. Perdew, J. P.; Burke, K.; Ernzerhof, M.; *Phys. Rev. Lett*., **1996**, *77*, 3865.
40. Andzelm, J.; King-Smith, R. D.; Fitzgerald, G.; *Chem. Phys. Lett.*, **2001**, *335*, 321.
41. Baker, J.; Kessi, A.; Delley, B.; *J. Chem. Phys.*, **1996**, *105*, 192.
42. Delley, B.; DMol, a standard tool for density functional calculations: Review and advances, In Modern Density Functional theory: A tool for Chemistry; Seminario, J. M.; Politzer, P. (Eds.); Theoretical and Computational Chemistry, Elsevier, **1995**, Vol. 2, pp. 221-254.
43. Weinert, M.; Davenport, J. W.; *Phys. Rev. B*, **1992**, *45*, 13709.
44. Mayer, I.; *Int. J. Quantum Chem.*, **1986**, *29*, 477.
45. Kakkar, R.; Grover, R.; Gahlot, P.; *Polyhedron*, **2006**, *25*, 759.
46. Singh, U. C.; Kollman, P. A.; *J. Comput. Chem.*, **1984**, *5*, 129.
47. Ao, Z. M.; Yang, J.; Li, S.; Jiang, Q.; *Chem. Phys. Lett.*, **2008**, *461*, 276.
48. Padak, B.; Wilcox, J.; *Carbon*, **2009**, *47*, 2855.
49. Dai, J.; Yuan, J.; *J. Phys.: Condens. Matter*, **2010**, *22*, 225501/1.
50. Allred, A. L.; *J. Inorg. Nucl. Chem.*, **1961**, *17*, 215.
51. Kakkar, R.; Grover, R.; Gahlot, P.; *J. Mol. Struct.: THEOCHEM*, **2006**, *767*, 175.
52. Kapoor, P. N.; Kakkar, R.; *J. Mol. Struct.: THEOCHEM.*, **2004**, *679*, 149.
53. Tyagi, P.; Gahlot, P.; Kakkar, R.; *Polyhedron*, **2008**, *27*, 3567.
54. Tang, Y.; Yang, Z.; Dai, X.; *J. Magn. Magn. Mater.*, **2011**, *323*, 2441.

